fluids

MDPI

Article

Modeling and Visualization of Coolant Flow in a Fuel Rod Bundle of a Small Modular Reactor

Sergei Dmitriev, Tatiyana Demkina, Aleksandr Dobrov, Denis Doronkov, Daniil Kuritsin, Danil Nikolaev, Alexey Pronin, Anton Riazanov * and Dmitriy Solntsev

The Department of the Nuclear and Thermal Power Stations, Institute of Nuclear Power Engineeniring and Applied Physics n.a. Academican F.M. Mitenkov, Nizhny Novgorod State Technical University n.a. R.E. Alekseev, 603950 Nizhny Novgorod, Russia; dmitriev@nntu.ru (S.D.); tatyana07041998@gmail.com (T.D.); dobrov@nntu.ru (A.D.); nevid000@mail.ru (D.D.); d.d.kuritsin@yandex.ru (D.K.); nikolaevdanil_ft@mail.ru (D.N.); proninaleksei@mail.ru (A.P.); solntsev@nntu.ru (D.S.)
* Correspondence: riazanov.av@nntu.ru

Abstract: This article presents the results of an experimental study of the coolant flow in a fuel rod bundle of a nuclear reactor fuel assembly of a small modular reactor for a small ground-based nuclear power plant. The aim of the work is to experimentally determine the hydrodynamic characteristics of the coolant flow in a fuel rod bundle of a fuel assembly. For this purpose, experimental studies were conducted in an aerodynamic model that included simulators of fuel elements, burnable absorber rods, spacer grids, a central displacer, and stiffening corners. During the experiments, the water coolant flow was modeled using airflow based on the theory of hydrodynamic similarity. The studies were conducted using the pneumometric method and the contrast agent injection method. The flow structure was visualized by contour plots of axial and tangential velocity, as well as the distribution of the contrast agent. During the experiments, the features of the axial flow were identified, and the structure of the cross-flows of the coolant was determined. The database obtained during the experiments can be used to validate CFD programs, refine the methods of thermal-hydraulic calculation of nuclear reactor cores, and also to justify the design of fuel assemblies.

Keywords: coolant; hydrodynamic; fuel assembly; reactor core; small modular reactor

Citation: Dmitriev, S.; Demkina, T.; Dobrov, A.; Doronkov, D.; Kuritsin, D.; Nikolaev, D.; Pronin, A.; Riazanov, A.; Solntsev, D. Modeling and Visualization of Coolant Flow in a Fuel Rod Bundle of a Small Modular Reactor. *Fluids* **2024**, *9*, 235. https://doi.org/10.3390/fluids9100235

Academic Editors: Mingming Ge and Tomoaki Kunugi

Received: 4 September 2024
Revised: 4 October 2024
Accepted: 5 October 2024
Published: 8 October 2024

1. Introduction

Rosatom, the State Atomic Energy Corporation Rosatom, is currently in the final stages of developing a modernized ground-based nuclear power plant that will generate electricity for remote and decentralized areas. For the modernized power unit, specialists from Rosatom have developed the RITM-200S small modular reactor (Nizhniy Novgorod, Russia). One of the main components of the reactor is the core. It is subject to increased demands for durability, energy efficiency, reliability, and safety. The new core uses fuel assemblies with an increased active part height of 1650 mm to extend the service life. It also uses fuel rods with a thicker cladding made from a corrosion-resistant alloy [1–4]. New technical solutions require experimental and computational justification. One of the stages in the design process for the core includes an experimental study of the hydrodynamics of the coolant inside the fuel rod bundle within a fuel assembly.

The main results of the thermophysical experiments were obtained by scientific teams that are part of the State Atomic Energy Corporation Rosatom and are published in [5]. These studies present the results of both experimental and computational research on critical heat flows in RITM-200 reactor fuel assemblies used in ground-based small modular nuclear power plants. All experiments were conducted under normal operating conditions of the reactor.

Also, complex analytical work is being conducted in scientific organizations to analyze the design and operational features of modernized small modular reactors. The works

in [6–9] present the results of analyzing the design of these reactors, identifying their weaknesses, analyzing their operating modes, and determining paths for their further modernization and development. It also includes recommendations for improving the design of the reactor core.

Scientists are mainly involved in the computational and experimental modeling of coolant hydrodynamics in PWR reactor cores. The main goal of these studies is to determine the influence of mixing grids and fuel bundle geometry on coolant flow processes. However, the influence of the geometry of mixing vanes on flow mixing and vortex formation in fuel bundles has not been thoroughly investigated, making it difficult to accurately assess the impact of these design features on flow patterns due to the complexity of processes in rod bundles, including the presence of secondary flows and turbulence anisotropy [10–14].

To identify the main patterns of coolant movement behind mixing grids, various approaches are used. These include the study of transverse mass transfer using tracer methods and laser Doppler technology, as well as the measurement of temperature fields in the coolant flow to gain a better understanding of dynamics [15,16].

In these studies, the focus is on the coolant flow within the fuel assembly, specifically the area behind the mixing grids. This area is represented by normal cells, formed by the arrangement of fuel rods, without any more complex cells such as peripheral regions, central displacer regions, or corner regions.

Accurate knowledge of the hydrodynamics of the coolant can help to improve the accuracy of results from thermohydraulic calculations for cores when justifying their reliability. Therefore, the aim of this work is to experimentally determine hydrodynamic characteristics of flow in fuel element bundles [17–26].

The results of experimental studies of the coolant hydrodynamics at the inlet and outlet, as well as in the fuel rod bundle of the fuel assembly for the core of the ground-based small modular reactor, are not available in the open press, which also confirms the relevance and scientific novelty of the results presented in this article.

2. Research Facility and Experimental Model

The flow of water coolant was simulated using airflow, based on the theory of hydrodynamic similarity, with the same Reynolds number in the range of 90,000 to 100,000 relative to the natural reactor unit. The open-circuit aerodynamic research facility consists of an airflow injection system and an experimental model equipped with a measurement system [27–31].

The experimental model is designed as a transparent hexagonal channel whose walls imitate the cover of a standard fuel assembly. The model's fuel bundle replicates the geometry of a fragment of a standard fuel assembly's fuel rod bundle and consists of fuel rod simulators and burnable absorber rods. In the fuel bundle, there are three spacer grid simulators installed. These simulators have a complex design, consisting of plates of different thicknesses and shapes. The central displacer simulator is located in the inner shells of the grids. The position of the grids in the model is based on their standard location, which has been enlarged by a scale factor. Six stiffening corners, which connect the grid simulators, are fixed to their outer shell and follow the geometry of the structural element of a standard fuel assembly (Figure 1). The scale factor for all elements in the experimental model is 5.8. By increasing the size of the design compared to the standard fuel assembly, we can reduce the impact of the probe sensors on the flow pattern. This solution also allows us to achieve a Reynolds number of 90,000 during low airflow velocities.

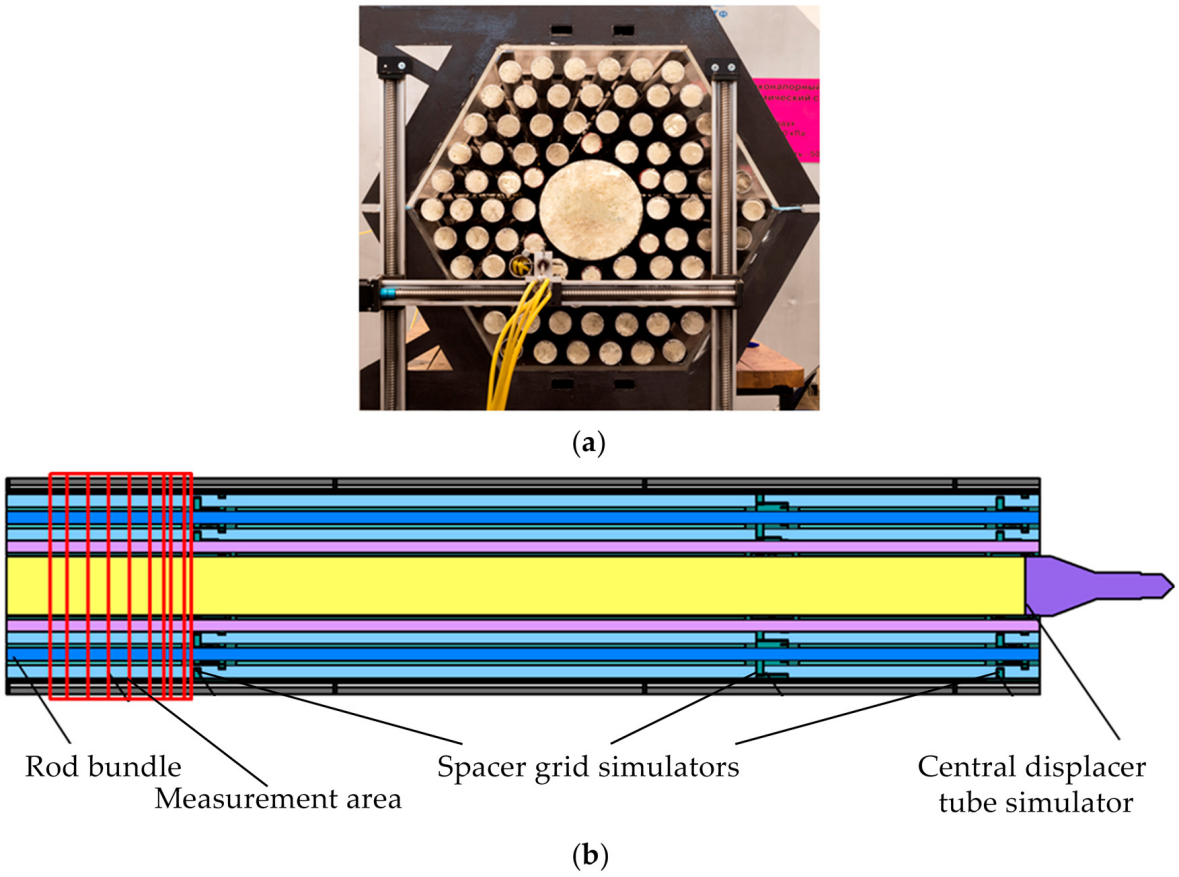

Figure 1. Model of a fuel rod bundle fragment: (**a**) External appearance of the experimental model, (**b**) Arrangement of structural elements in the experimental model channel.

3. The Representativeness of the Study

When performing hydrodynamic similarity, it is possible to choose the optimal design of the experimental model and recalculate the flow characteristics obtained during experiments for the natural conditions of coolant flow. This is achieved by ensuring geometric, kinematic, and dynamic similarity between the model and actual construction.

Geometric similarity is maintained by matching the geometric dimensions of the experimental model and the real object, taking into account scale factors.

The dynamic similarity of the flow of fluid in geometrically similar objects can be observed due to the close values of the Reynolds number. The maximum Reynolds number in the experimental model is 90,000, and in the reference object, it is 100,000.

The kinematic similarity of flows in geometrically similar objects is observed due to the proportionality of dimensionless velocities at the corresponding points of the experimental model and the real object.

The value of the Reynolds number, which was used in the research, corresponds to the range of self-similarity of flow, which allows us to use experimental data to study the flow of water coolant. The start of the self-similar zone is defined by a Reynolds number of 35,000. All measurements were taken at an average air velocity of 36.2 m/s at the entrance to the model with a Reynolds of 90,000

Additionally, the representativeness of the experiments is proved by the agreement between the hydraulic resistance coefficients of the test grids and those of standard design elements, which have identical Reynolds numbers.

4. Experimental Methodology

The hydrodynamic properties of the flow within a fuel bundle were studied using the pneumometry approach and the technique of impurity injection.

A multi-hole pressure probe has been used to measure the velocity vector in an experimental model. The sensitive part of the probe consists of five steel capillaries with a diameter of 0.8 × 0.1 mm, located in two perpendicular diametric planes. The rest of the capillaries are placed inside a steel tube that serves as the probe holder. The central capillary is cut at a 90-degree angle to its axis, while the four lateral capillaries are cut at a 45-degree angle (Figure 2).

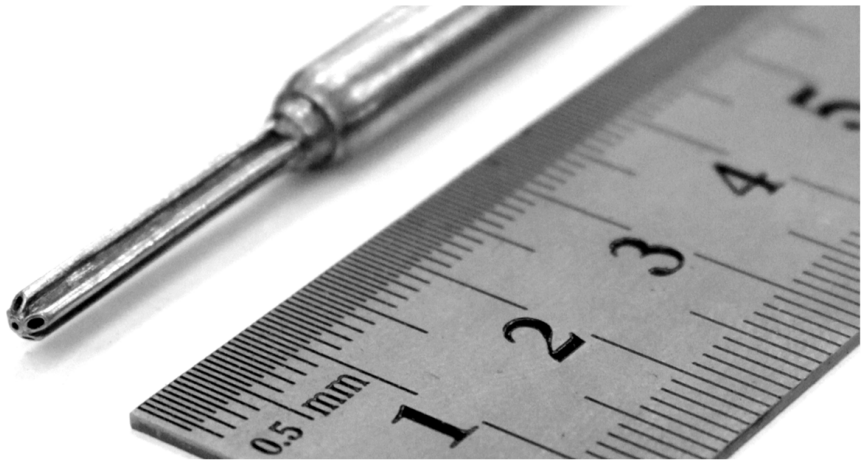

Figure 2. Multi-hole pressure probe.

To measure the magnitude and direction of the velocity vector, a pneumatic probe is sequentially positioned at specific points on the experimental fuel assembly model using a coordinate system. In this process, pressure values in each capillary of the probe are recorded using piezoelectric pressure sensors.

Flow velocity components were measured with an accuracy of not more than 7.5% error.

The structure of transverse flows was investigated using the injection method with the addition of propane. This gas was injected at a specific flow rate into areas located in front of the third grate along the flow path. After injection, the distribution of the added substance in the volume of the model was monitored using an infrared gas analyzer. The gas flow rate was maintained with an accuracy of ±0.25%. The impurity concentration levels were determined using a gas analyzer with an error of ±1.5% or lower.

The size of the measuring area is determined by the large number of cells of various shapes and by the geometry of the spacers, which intersect in various ways. This area occupies one-third of the cross-sectional area of the fuel bundle and has a significant number of impurity entry points (Figure 3). The flow velocity components and impurity concentrations were measured across the entire area of interest using a uniform grid of measurement points. Along the length of the rod bundle, measurements were taken at 10 sections behind the simulator of the third spacer grid. The distance between these measurement points increased as the distance from the grid increased (Figure 1). This choice of measurement area size and placement of impurity injection points allows us to characterize the overall flow structure.

The analysis of the coolant flow was conducted based on contour plots of the dimensionless impurity concentration and the flow velocity. The values of the dimensionless axial (W_z/W_{av}) and tangential (W_{xy}/W_{av}) velocities were obtained by dividing their local values at a point by the value of the average flow velocity at the inlet of the experimental model (W_{av}). The values of the dimensionless impurity concentration (C/C_0) are calculated by dividing its local value (C) at a given point by the maximum value of the impurity concentration in the injection region immediately in front of the spacer grid (C_0). To estimate the flow disturbances caused by the structural elements in the experimental model, we

used the value L/d_h, where L is the distance from the measurement point to the structure, and d_h is the hydraulic diameter of the model.

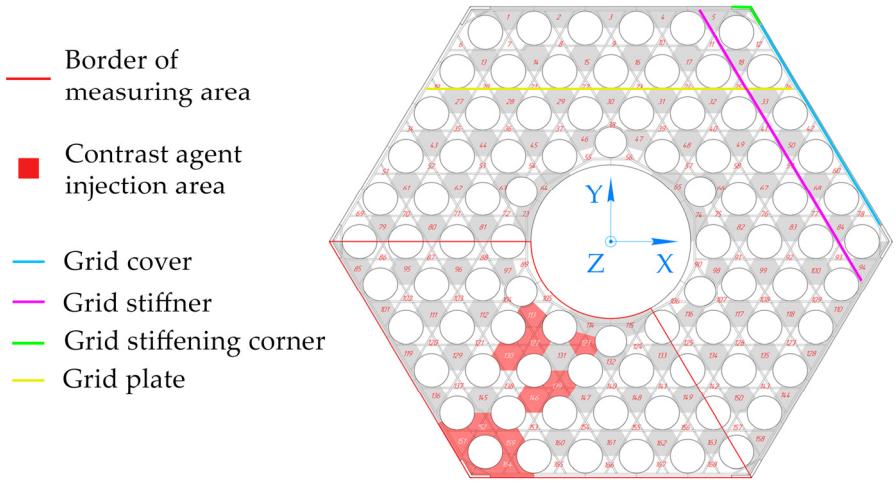

Figure 3. The location of the measuring area and contrast agent injection zones in the cross-section of the experimental model.

5. The Results of the Study on the Hydrodynamics of the Coolant Using the Pneumometry Technique

In the field of regular cells, transverse flows were formed behind the plates and grid stiffeners at the points of their contact with the fuel elements at a distance of $L/d_h \approx 1$ (Figure 4) from the spacer grid. Behind the stiffeners, the dimensionless tangential velocity was 0.17–0.22, and behind the plates, it was two times less, which is due to their smaller thickness. The transverse flow maintained its structure up to a distance of approximately three times the hydraulic diameter ($L/d_h \approx 3.1$) from the plates.

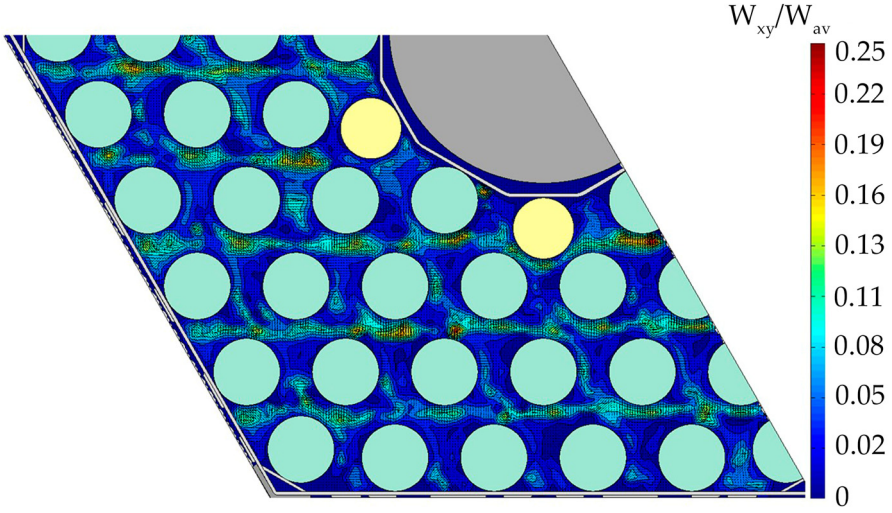

Figure 4. Dimensionless tangential flow velocity at a distance of $L/d_h \approx 1$ from the grid simulator plates.

At the faces of the fuel assembly cover and the stiffening corners, where there were no grid plates, the transverse flow was oriented from regular cells towards the outer edges. However, at the intersection of plates, the direction of transverse flow is reversed. Dimensionless tangential velocities ranged from 0.08 to 0.13 in the first case and 0.11–0.14 in the second case. In the case without plates in the cells, the transverse flow stopped at $L/d_h \approx 7.5$. In the case of the plates intersecting cells, it stopped at a distance of $L/d_h \approx 5$.

Near the central displacer, transverse flow moved across the surface of the displacer in a circular pattern, as well as within a field of regular cells located at a distance of $L/d_h \approx 2$ from the plates. These transverse flows were measured throughout the entire research area. In transverse flows moved around the central displacer, the dimensionless tangential velocity ranged from 0.13 to 0.16. In transverse flows directed into the field of regular cells, the dimensionless tangential velocity ranged from 0.11 to 0.13 (Figure 5).

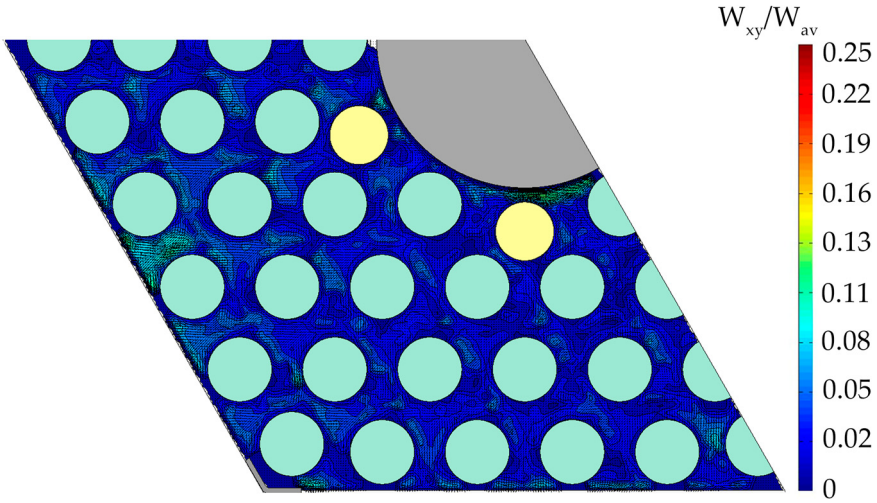

Figure 5. Dimensionless tangential flow velocity at a distance of $L/d_h \approx 2$ from the grid simulator plates.

In regular cells, with no grid plates in the center, the structure of the axial velocity profile had a uniform structure. The dimensionless axial velocity at distances $L/d_h \approx 1$ and $L/d_h = 10$ from the plate ranged from 1.1 to 1.2 and from 0.9 to 1, respectively. In regular cells with intersecting plates in the center, the axial flow was non-uniform. The dimensionless velocity ranged from 0.5 to 0.9. Behind the grid plate profiles, in areas where they contacted fuel elements and between fuel rods, axial flow velocity was minimal. The highest velocities were found in free areas of cells. At the points of the local minimum and maximum, the dimensionless axial velocity ranged from 0.5 to 0.7 and 0.8 to 0.9, respectively. Homogenization of the axial flow velocity in the field of regular cells occurred at a distance of $L/d_h \approx 10$ from the grid (Figures 6 and 7).

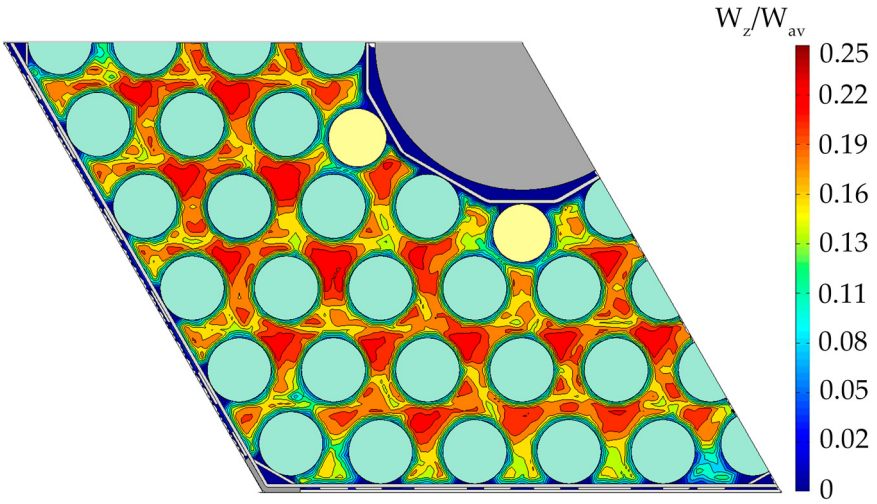

Figure 6. Dimensionless axial flow velocity at a distance of $L/d_h \approx 1$ from the grid simulator plates.

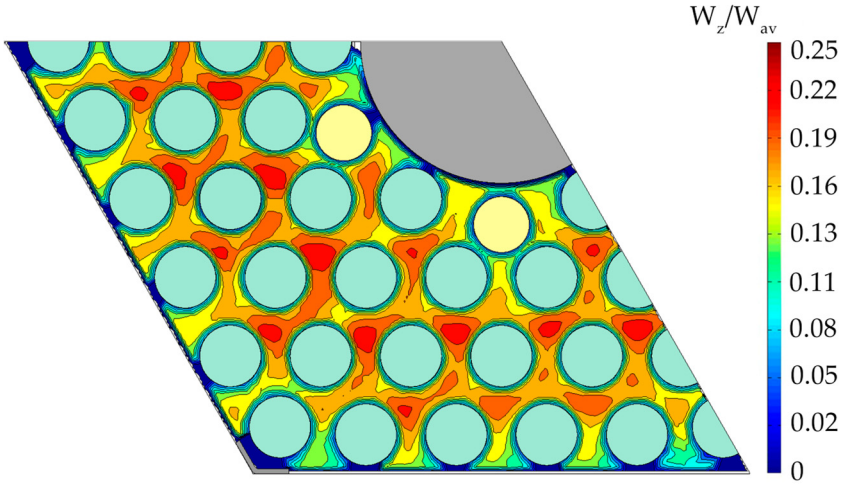

Figure 7. Dimensionless axial flow velocity at a distance of $L/d_h \approx 10$ from the grid simulator plates.

Near the fuel assembly cover, the flow velocity was lower than in the field of regular cells. The dimensionless velocity at a distance of $L/d_h \approx 1$ from the plates ranged from 0.3 to 0.9.

The axial flow velocity in the peripheral cells, remote from the stiffening corners, was influenced by the arrangement of the grid plates. At a distance of $L/d_h \approx 1$ from the grid, the dimensionless velocity in the cells without plates ranged from 0.8 to 0.9 and with plates from 0.4 to 0.75. At a larger distance of $L/d_h \approx 10$, velocities ranged from 0.9 to 1 without plates and from 0.5 to 0.8 with plates, indicating a lower intensity of flow velocity field equalization (Figures 6 and 7). The lowest flow velocity in the corner cells with grid plates in the center ranged from 0.3 to 0.6 at a distance of $L/dh \approx 1$ and from 0.4 to 0.7 at a distance of $L/d_h \approx 10$. In the corner cells without plates, the dimensionless axial flow velocity was higher. At distances of $L/d_h \approx 1$, it ranged from 0.6 to 0.8, and at distances of $L/d_h \approx 10$, it ranged from 0.8 to 0.9.

The speed of the axial flow was higher near the center of the displacer than at the periphery. Its dimensionless value ranged from 0.8 to 1.1 at distances $L/d_h \approx 1$ from the grid plates and from 0.75 to 0.9 at distances $L/d_h \approx 10$ (Figure 5).

6. The Results of the Study on the Hydrodynamics of the Coolant Using the Contrast Agent Injection Method

In the area of regular cells, which are located away from the central displacer tube and the fuel assembly cover, the transverse flow between the cells and the mixing of the coolant were low-intensity. The design of the spacer grid plates had a minimal impact on the process of cooling in regular cells. This is confirmed by the similarity in the distribution of impurities shown in Figure 8.

The flow in the area of regular cells near the central displacer tube is influenced by transverse flows from the displacer region. This is confirmed by the asymmetry in the distribution of the contrast agent, as shown in the contour plots in Figure 9.

In the peripheral cells, where the grid plates intersect, the transverse flow was oriented within the regular cells. There was no movement of coolant across the surface of the fuel assembly cover in a transverse direction. No reverse transverse flows were recorded from regular cells to peripheral cells (Figure 10). In peripheral cells without a plate intersection, transverse flows were oriented in the opposite direction from regular cells towards the periphery. Transverse flow of coolant along the surface of the fuel assembly cover was also observed. The presence of reverse flow from regular cells to the periphery has also been recorded (Figure 11).

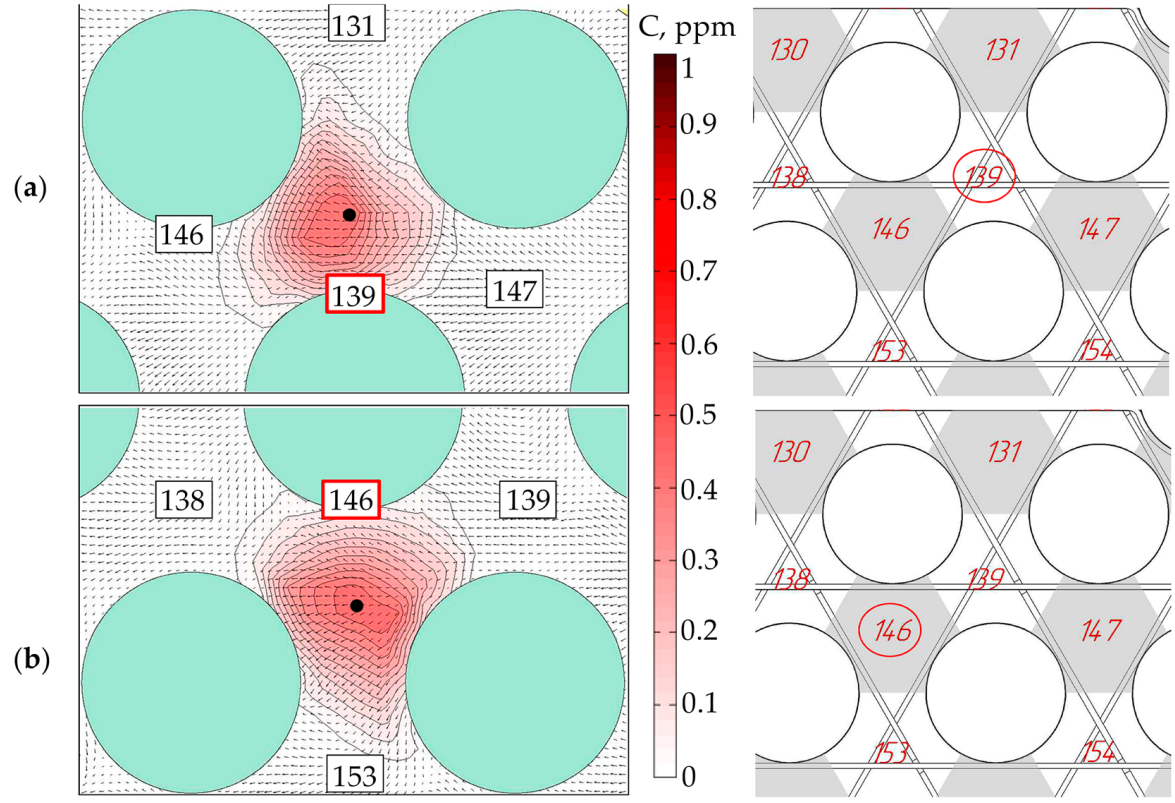

Figure 8. Contour plots of contrast agent distribution in regular cells: (**a**) Regular cell with plate intersection; (**b**) Regular cell without plate intersection.

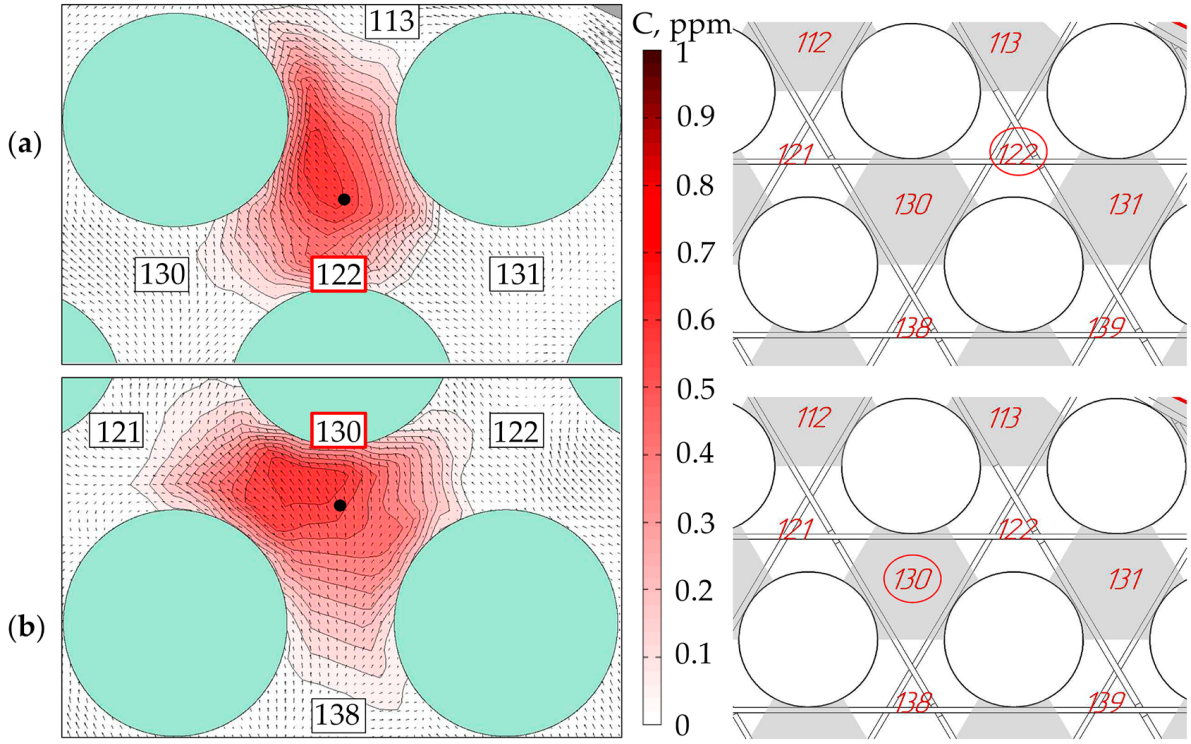

Figure 9. Contour plots of contrast agent distribution in regular cells: (**a**) Regular cell with plate intersection; (**b**) Regular cell without plate intersection.

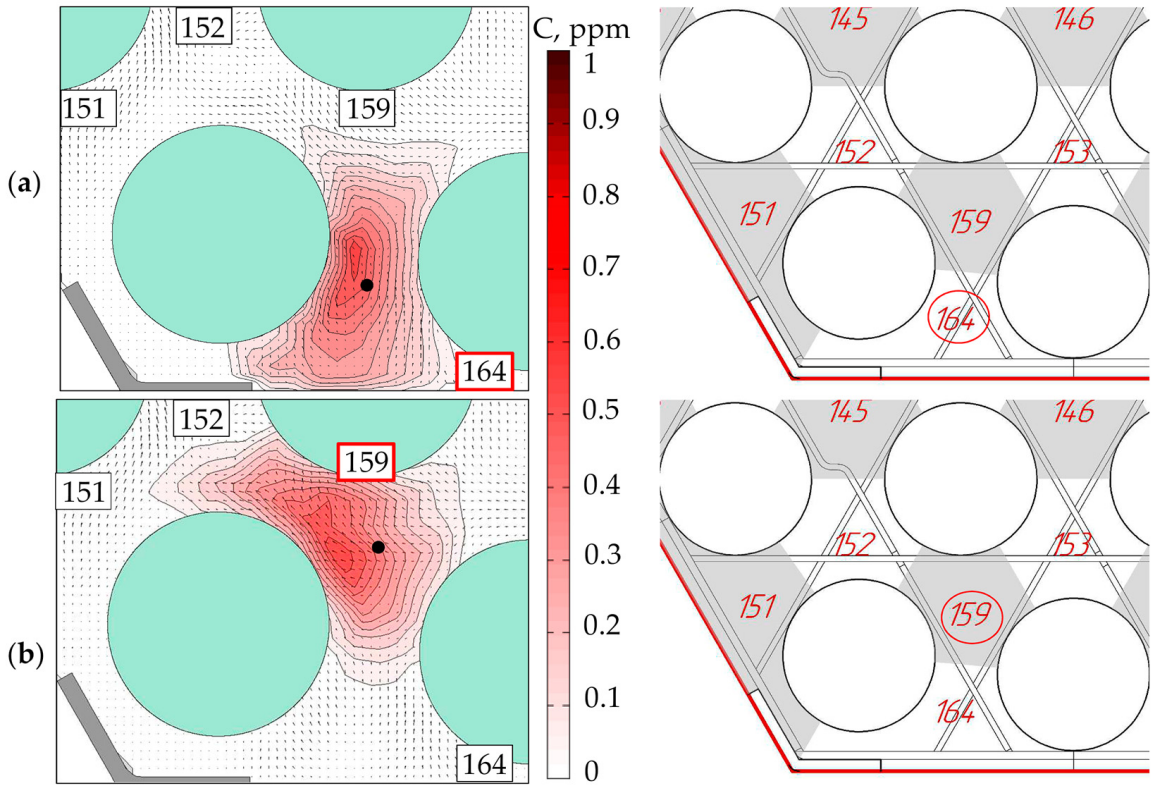

Figure 10. Contour plots of contrast agent distribution near the fuel assembly cover: (**a**) Cell with a plate intersection; (**b**) Cell without a plate intersection.

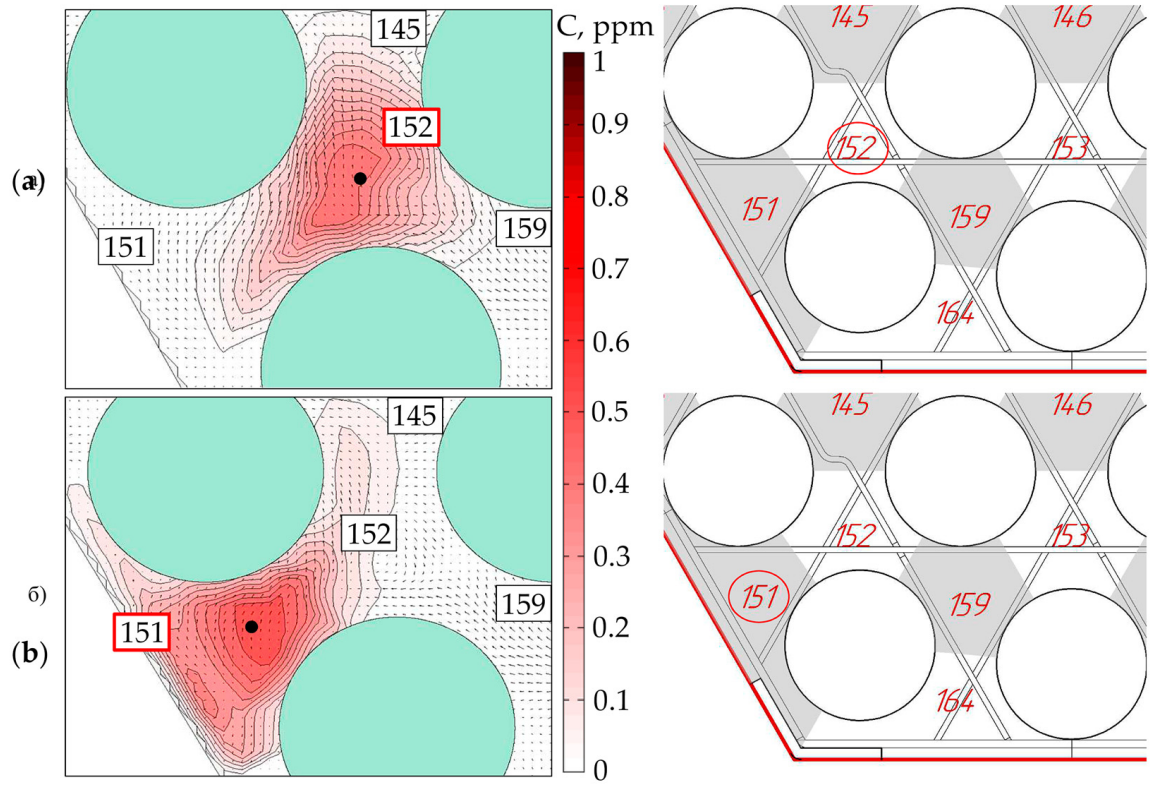

Figure 11. Contour plots of contrast agent distribution near the fuel assembly cover: (**a**) Cell with a plate intersection; (**b**) Cell without a plate intersection.

The flow of the coolant near the central displacer was determined by the transverse circular flow that was directed along its surface. This circular flow carried away some of the axial flow of the coolant from the cells near the displacer tube. The structure of the coolant flow is shown in the contour plot in Figure 12.

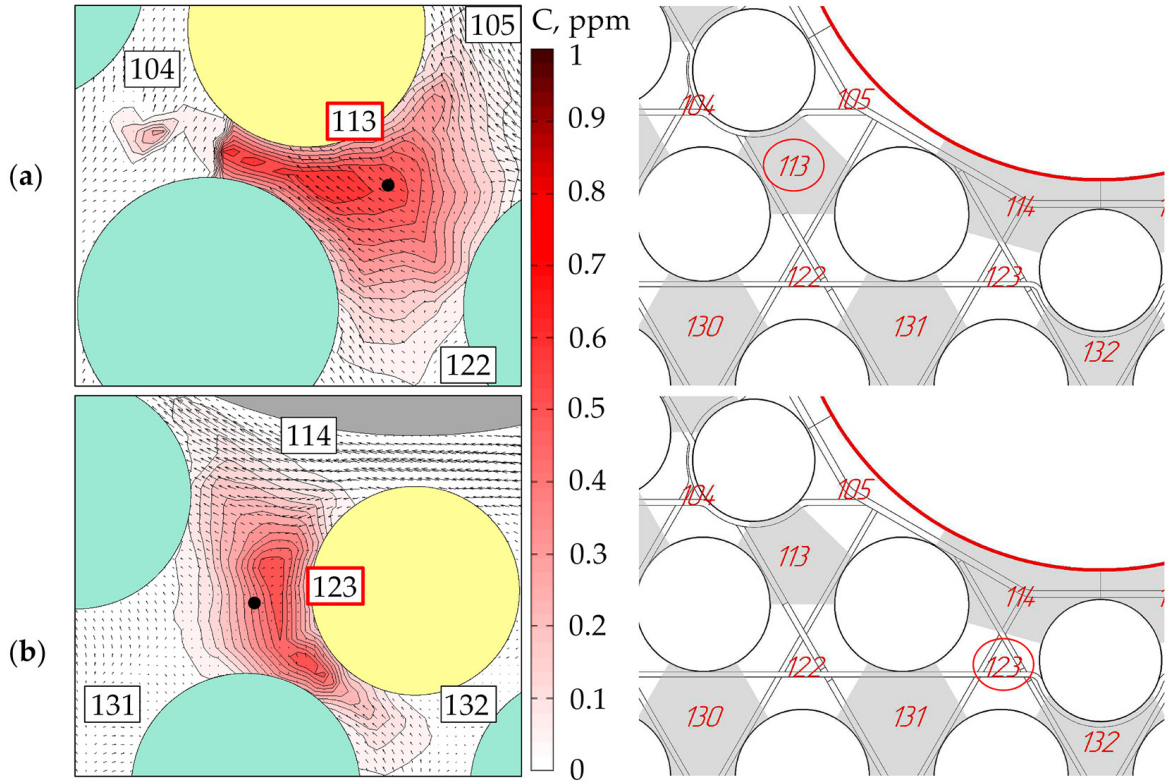

Figure 12. Contour plots of contrast agent distribution near the central displacer tube: (**a**) Cell with a plate intersection; (**b**) Cell without a plate intersection.

7. Discussion

In the fuel assembly, the coolant flow is significantly non-uniform due to the complex geometry of the fuel assembly bundle and spacer grids, as well as the presence of the fuel assembly cover, central displacer tube, and stiffening corners.

At the fuel assembly cover, the axial flow has the lowest velocities. The local minimum of the axial velocity is recorded in the areas around the stiffening corners. The average dimensionless velocity ranges from 0.3 to 0.7. The process of equalizing the axial flow velocity between the corner areas and the areas of regular cells is slow.

Behind the grid plates, the axial flow in the area of regular cells is non-uniform. The alignment of the axial flow structure in regular cells occurs at a distance of $L/d_h \approx 10$ from the grid plates.

At the central displacer tube, the axial flow velocity decreases, and its dimensionless value ranges from 0.75 to 0.9. This is due to the transverse flow directed towards the field of regular cells.

In the axial flow structure, three different regions can be identified with velocity values that differ by 25–30%. These are regular cells, the displacement region, and the peripheral region.

The arrangement of the grid plates has a significant effect on the structure of the axial flow in all areas of the fuel rod bundle and on the formation of transverse coolant flows only in the peripheral area near the fuel assembly cover.

The identified features of the coolant flow should be taken into account when justifying heat engineering reliability using one-dimensional calculation codes.

It is necessary to modernize one-dimensional calculation codes by increasing the number of cell types and considering the non-uniformity of flow through fuel bundle regions as well as different cell types. Additionally, it is important to update the coolant mixing matrix based on results from experimental studies using a contrast agent injection method.

Author Contributions: Conceptualization, S.D.; methodology, D.D. and A.P.; investigation, D.K. and D.N.; formal analysis, A.D. and A.R.; writing—original draft preparation, A.R.; writing—review and editing, D.D. and A.R.; visualization, T.D. and A.P.; software, A.D. and A.R.; supervision, S.D.; project administration, D.D.; funding acquisition, D.S. All authors have read and agreed to the published version of the manuscript.

Funding: This research was funded by the Ministry of Science and Higher Education of the Russian Federation (project No. FSWE-2024-0003).

Data Availability Statement: The original contributions presented in the study are included in the article, further inquiries can be directed to the corresponding author.

Conflicts of Interest: The authors declare no conflicts of interest.

References

1. Petrunin, V.V.; Sheshina, N.V.; Fateev, S.A.; Kurachenkov, A.V.; Shchekin, D.V.; BrykaloV, S.M.; Bezrukov, A.A. Scientific and technical aspects of developing a RITM-200N innovative reactor for SNPPs. *At. Energy* **2023**, *134*, 1–10. [CrossRef]
2. Filippov, S.P.; Veselov, F.V.; Pankrushina, T.G. Prospects of SNPPs in the electric power industry. *At. Energy* **2023**, *134*, 11–20. [CrossRef]
3. Zverev, D.L.; Fadeev, Y.P.; Pakhomov, A.N.; Galitskikh, V.Y.; Polunichev, V.I.; Veshnyakov, K.B.; Kabin, S.V.; Turusov, A.Y. Reactor Installations for Nuclear Icebreakers: Origination Experience and Current Status. *At. Energy* **2020**, *129*, 18–26. [CrossRef]
4. Belyaev, V.M.; Bol'shukhin, M.A.; Pakhomov, A.N.; Khizbullin, A.M.; Lepekhin, A.N.; Polunichev, V.I.; Veshnyakov, K.B.; Sokolov, A.N.; Turusov, A.Y. The World's First Floating NPP: Origination and Direction of Future Development. *At. Energy* **2020**, *129*, 27–34. [CrossRef]
5. Zakharychev, A.A.; Iksanova, G.S.; Kupriyanov, A.V.; Osin, A.B.; Petrunin, V.V.; Samoilov, O.B.; Shipov, D.L. Methodological Issues and Results of Experimental and Computational Studies of Critical Heat Flows in RITM-200 Reactor Fuel Assemblies for Small NPP. *At. Energy* **2021**, *130*, 63–68. [CrossRef]
6. Korolev, V.I. Analysis of New Technical Solutions for the RITM-200 Reactor Plant in Project 22220 Universal Nuclear Icebreakers. *Vestn. Gos. Univ. Morskogo Rechn. Flot. Im. Admirala S. O. Makarova* **2022**, *14*, 945–960. [CrossRef]
7. Tan, S.; Cheng, S.; Wang, K.; Liu, X.; Cheng, H.; Wang, J. The development of micro and small modular reactor in the future energy market. *Front. Energy Res.* **2023**, *11*, 1149127. [CrossRef]
8. Crețulescu, A. Small Modular Reactors in Romania's Energy Future. Two Essential Perspectives: Capital Costs and Public Perception. *Proc. Int. Conf. Bus. Excell.* **2024**, *18*, 1765–1775. [CrossRef]
9. Deng, C.; Zhu, S.; He, Y.; Wu, Y.; He, K.; Zhang, J.; Su, G. Analysis of Gas-Cooled Micro Modular Reactor (MMR) Fuel. *J. Nucl. Mater.* **2024**, *598*, 155191. [CrossRef]
10. Trupp, A.C.; Azad, R.S. The Structure of Turbulent Flow in Triangular Array Rod Bundles. *Nucl. Eng. Des.* **1975**, *32*, 47–84. [CrossRef]
11. Caraghiaur, D. *Experimental Study and Modeling of Spacer Grid Influence on Flow in Nuclear Fuel Assemblies*; Technical Report; KTH Stockholm: Stockholm, Sweden, 2009.
12. Bakosi, J.; Christon, M.A.; Lowrie, R.B.; Pritchett-Sheats, L.A.; Nourgaliev, R.R. Large-eddy simulations of turbulent flow for grid-to-rod fretting in nuclear reactors. *Nucl. Eng. Des.* **2013**, *262*, 544–561. [CrossRef]
13. Peña-Monferrer, C.; Muñoz-Cobo, J.L.; Chiva, S. CFD turbulence study of PWR spacer-grids in a rod bundle. *Sci. Technol. Nucl. Install.* **2014**, *2014*, 635651. [CrossRef]
14. Sergeev, D.A.; Kandaurov, A.A.; Troitskaya, Y.I. The particular use of PIV methods for the modelling of heat and hydrophysical processes in the nuclear power plants. *J. Phys. Conf. Ser.* **2017**, *891*, 012088. [CrossRef]
15. Yu, H.; Cai, J.; He, S.; Li, X. Analysis of neutron physics and thermal hydraulics for fuel assembly of small modular reactor loaded with ATFs. *Ann. Nucl. Energy* **2020**, *152*, 107957. [CrossRef]
16. He, S.; Cai, J.; Chen, Z.; Liu, R. Thermal hydraulic analysis of accident tolerant fuels for Reactivity-Initiated-Accident in PWR with different coolant channel geometries. *Nucl. Eng. Des.* **2019**, *351*, 131–142. [CrossRef]
17. Cong, T.; Zhang, X. Numerical Study of Bubble Coalescence and Breakup in the Reactor Fuel Channel with a Vaned Grid. *Energies* **2018**, *11*, 256. [CrossRef]
18. Tian, Z.; Yang, L.; Han, S.; Yuan, X.; Lu, H.; Li, S.; Liu, L. Numerical Investigation on the Flow Characteristics in a 17 × 17 Full-Scale Fuel Assembly. *Energies* **2020**, *13*, 397. [CrossRef]
19. Lee, I.S.; Yoon, D.H.; Bang, Y.S.; Kim, T.H.; Kim, Y.C. Assessment of Realistic Departure from Nucleate Boiling Ratio (DNBR) Considering Uncertainty Quantification of Core Flow Asymmetry. *Energies* **2021**, *14*, 1504. [CrossRef]

20. Vlasov, M.N.; Merinov, I.G. Application of an Integral Turbulence Model to Close the Model of an Anisotropic Porous Body as Applied to Rod Structures. *Fluids* **2022**, *7*, 77. [CrossRef]
21. Kim, K.; Kim, W.-S.; Choi, H.-S.; Seol, H.; Lim, B.-J.; Euh, D.-J. An Experimental Evaluation of the APR1000 Core Flow Distribution Using a 1/5 Scale Model. *Energies* **2024**, *17*, 2714. [CrossRef]
22. Beliavskii, S.; Alhassan, S.; Danilenko, V.; Karvan, R.; Nesterov, V. Effect of changing the outer fuel element diameter on ther-mophysical parameters of KLT-40S reactor unit. *Ann. Nucl. Energy* **2023**, *190*, 109877. [CrossRef]
23. Hidayatullah, H.; Susyadi, S.; Hadid Subki, M. Design and technology development for small modular reactors—Safety expectations, prospects and impediments of their deployment. *Prog. Nucl. Energy* **2015**, *79*, 127–135. [CrossRef]
24. Bhowmik, P.K.; Sabharwall, P.; Johnson, J.T.; Retamales, M.E.T.; Wang, C.; O'Brien, J.E.; Lietwiler, C.; Wu, Q. Scaling methodologies and similarity analysis for thermal hydraulics test facility development for water-cooled small modular reactor. *Nucl. Eng. Des.* **2024**, *424*, 113235. [CrossRef]
25. Ren, L.; Minjun, P.; Genglei, X.; Lin, S. The natural circulation flow characteristic of the core in floating nuclear power plant in rolling motion. *Ann. Nucl. Energy* **2020**, *142*, 107385. [CrossRef]
26. Alam, S.B.; de Oliveira, R.G.G.; Goodwin, C.S.; Parks, G.T. Coupled neutronic/thermal-hydraulic hot channel analysis of high power density civil marine SMR cores. *Ann. Nucl. Energy* **2019**, *127*, 400–411. [CrossRef]
27. Samoilov, O.B.; Shipov, D.L.; Kupriyanov, A.V.; Sholin, E.V.; Vishneva, T.Y.; Molodtsov, A.A.; Osin, A.B.; Dmitriev, S.M.; Khrobostov, A.E.; Doronkov, D.V.; et al. Efficiency studies of heat-transfer intensifier grids in TVSA-T model fuel assemblies. *At. Energy* **2020**, *128*, 17–23. [CrossRef]
28. Dmitriev, S.M.; Gerasimov, A.V.; Dobrov, A.A.; Doronkov, D.V.; Pronin, A.N.; Solntsev, D.N.; Khrobostov, A.E.; Shvetsov, Y.K.; Shipov, D.L. Hydrodynamics and mixing of a coolant in the core of the VVER with fuel assemblies of different designs. *Thermophys. Aeromech.* **2019**, *26*, 845–860. [CrossRef]
29. Gerasimov, A.V.; Dmitriev, S.M.; Dobrov, A.A.; Doronkov, D.V.; Pronin, A.N.; Ryazanov, A.V.; Solntsev, D.N.; Khrobostov, A.E. Computational-experimental investigations of the processes of motion of a coolant flow in the region of the guide channel behind mixing grids of fuel assemblies. *J. Eng. Phys. Thermophys.* **2020**, *93*, 145–154. [CrossRef]
30. Samoilov, O.B.; Noskov, A.S.; Shipov, D.L.; Dmitriev, S.M.; Dobrov, A.A.; Doronkov, D.V.; Legchanov, M.A.; Pronin, A.N.; Solntsev, D.N.; Sorokin, V.D.; et al. Hydrodynamic features of the flow downstream from the mixing spacer grid in a Kvadrat fuel assembly in PWRs. *Therm. Eng.* **2019**, *66*, 243–248. [CrossRef]
31. Dmitriev, S.M.; Dobrov, A.A.; Doronkov, D.V.; Doronkova, D.S.; Legchanov, M.A.; Pronin, A.N.; Ryazanov, A.V.; Khrobostov, A.E. Studies of the hydrodynamics of the coolant behind the mixing intensifier grids of the fuel assemblies of a PWR reactor. *High Temp.* **2022**, *60*, 358–365. [CrossRef]